# Improved Hypothesis Selection for Multiple Hypothesis Tracking

Juan R. Vasquez[a] and Jason L. Williams[b,c]

[a]Air Force Office of Scientific Research, Arlington, VA 22203, USA
[b]Department of Electrical and Computer Engineering, Air Force Institute of Technology, 2950 Hobson Way, Wright-Patterson Air Force Base, OH 45433, USA
[c]Department of Electrical Engineering and Computer Science, Massachusetts Institute of Technology, 77 Massachusetts Avenue, Cambridge, MA 02139, USA

## ABSTRACT

The need to track closely-spaced targets in clutter is essential in support of military operations. This paper presents a Multiple Hypothesis Tracking (MHT) algorithm which uses an efficient structure to represent the dependency which naturally arises between targets due to the joint observation process, and an Integral Square Error (ISE) mixture reduction algorithm for hypothesis control. The resulting algorithm, denoted MHT with ISE Reduction (MISER), is tested against performance metrics including track life, coalescence and track swap. The results demonstrate track life performance similar to that of ISE-based methods in the single-target case, and a significant improvement in track swap metric due to the preservation of correlation between targets. The result that correlation reduces the track life performance for formation targets requires further investigation, although it appears to demonstrate that the inherent coupling of dynamics noises for such problems eliminates much of the benefit of representing correlation only due to the joint observation process.

**Keywords:** Multiple Hypothesis Tracking (MHT), multiple target tracking, Gaussian mixture reduction, Integral Square Error, optimal filtering

## 1. INTRODUCTION

The goal of tracking multiple targets in random clutter presents significant problems for many tracking algorithms, including track coalescence, track swap, and loss of track. This paper presents a Multiple Hypothesis Tracking (MHT) algorithm which attempts to address these challenges using an efficient structure to represent the correlation which naturally arises between targets, and the Integral Square Error (ISE) mixture reduction algorithm[1–3] for hypothesis control.

For illustration purposes, consider the two-target example shown in Figure 1, where measurements $m_1$ and $m_2$ fall within the association gate of target $t_1$ and measurements $m_1, m_2$ and $m_3$ fall within the gate of target $t_2$. Each measurement falling within the gate of a target will form a new single-target hypothesis, alongside the hypothesis under which the detection of the target was missed, represented through association with the symbolic measurement $m_0$ (no measurement). A single target association hypothesis would be that $m_1$ is associated with $t_1$, or that $m_3$ is associated with $t_2$. Each single target association event would have a probability, a mean state estimate and accompanying covariance.

Joint association events combine single-target association events for each target in the cluster to provide a globally consistent view of measurement-to-target associations, where consistency denotes that each target is associated with (at most) a single measurement, and each measurement is associated with (at most) a single target. With each new scan of measurement data comes a new set of association hypotheses that must be paired with the association events of the previous processing cycle. This leads to a Gaussian mixture representation of the PDF of the target state vector, with the number of components in the mixture growing exponentially with

Further author information: (Send correspondence to J.R.V.)
J.R.V.: Telephone: +1 (703) 696-8431
J.L.W.: Telephone: +1 (617) 253-7220

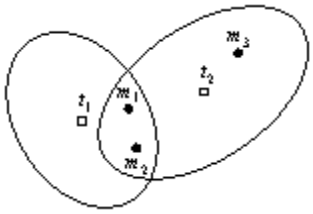

**Figure 1.** Two-target data association example

time, hence any practical implementation must include a method of simplifying the representation. The ISE-based mixture reduction algorithm has been shown to provide a significant performance advantage over traditional methods for relatively small numbers of components,* hence it is adopted for this study. Our algorithm will be referred to as MISER (MHT with ISE Reduction).

It is well-known that, as targets become closely spaced, the joint observation process of sensors with unlabeled data induces dependency between targets in the joint PDF of target state. The way that this dependency is represented has a significant impact on the way in which hypothesis reduction is performed. If hypothesis reduction is performed directly on the joint PDF of target state, merging and pruning joint association hypotheses, then the merging operations will result in a unique joint mean vector and covariance matrix for each joint association hypothesis, potentially including coupling between the targets. Since the number of joint association events increases combinatorially with the number of targets, this is highly undesirable.

In this study we seek to represent this dependency efficiently through a joint association event probability matrix. By isolating the dependency to this structure, we are able to avoid the burden of joint mean vectors and covariance matrices, instead maintain a series of mean vectors and covariance matrices for each target (single target hypotheses), and forming joint association events out of these single target blocks. We test whether the correlation represented through the joint association probability matrix will provide useful information in the next processing cycle versus maintaining a marginalized representation. MHT algorithms inherently keep track of this correlation; however, algorithms such as the Structured Branching MHT (SB-MHT)[4] simply employ hypothesis pruning, making the mathematics of the joint probability information easy to manage. In the case of hypothesis merging, this management becomes more complicated as discussed in the description of the MISER algorithm.

The problem examined is that of track maintenance, utilizing a set of measurements to update a group of previously-established targets. Track initiation and deletion are not considered; rather it is assumed that the number of target is known. In this respect, MISER may be referred to more as a mixture reduction or Gaussian sum filter approach, than a classical MHT. It is closely related to the Multisensor Multitarget Mixture Reduction (MTMR) algorithms,[5] with the major distinctions being the use of the ISE-based hypothesis reduction techniques, and the correlated representation. The remainder of this paper will present the details of the MISER algorithm, discuss the results and analysis of various two-target scenarios, then end with concluding remarks.

## 2. ALGORITHM

The following is a brief overview of the steps involved in generating a combined estimate of the target state via the joint target state PDF denoted as $f\{\mathbf{X}(k)|\mathbf{Z}^k\}$. The notation of capital $\mathbf{Z}(k)$ is used to represent the set of all measurements received at time $k$, $\mathbf{Z}^k$ represents all measurements received up to and including time $k$, and $\mathbf{X}(k)$ represents the joint target state variable. First, measurements within the gate of the current set of hypotheses for each target are used to generate new single target hypotheses (tracks), including the hypothesis of a missed detection. Each hypothesis includes a mean vector and covariance matrix. Assuming that the number of targets (T) is known, the joint target state PDF incorporating the new measurement information is represented through a T-dimensional joint hypothesis probability array, where the length of each dimension equal to the number new

*i.e., between 10 and 100.

single target hypotheses. The elements of this table weight products of single-target hypotheses to form the joint target state PDF.

This joint hypothesis probability array is then marginalized to find the marginal hypothesis probability for each target. The combined tracks or state estimates (mean and covariance) are generated from each single target hypothesis mean and covariance, appropriately weighted by the marginal probabilities. In order to keep the algorithm tractable, hypothesis reduction (merging and pruning) is conducted based on the marginal probabilities, generating new Gaussian mixtures with a smaller number of components. Based on the decisions made within the hypothesis reduction method, the marginal and joint hypothesis probabilities are modified as inputs to the next sample period along with their associated mean and covariance values. The approach allows correlation between single target hypotheses to be maintained through the joint hypothesis probability array. A 2-dimensional example will be used to illustrate many of the concepts being presented.

### 2.1. Forming the joint PDF and marginal probabilities

First, assume a linear dynamics model with state, $\mathbf{x}^t(k)$, evolving for each target $t$ at sample time $k$ based on the following:

$$\mathbf{x}^t(k) = \mathbf{\Phi}^t(k, k-1)\mathbf{x}^t(k-1) + \mathbf{G}_d^t(k-1)\mathbf{w}^t(k-1) \tag{1}$$

$$\mathbf{z}_{l_t}(k) = \mathbf{H}^t(k)\mathbf{x}^t(k) + \mathbf{v}^t(k) \tag{2}$$

where $\mathbf{z}_{l_t}(k)$ is the noise corrupted measurement originating from the true target and provided to the estimator; $\mathbf{\Phi}^t, \mathbf{G}_d^t$, and $\mathbf{H}^t$ are known system matrices; $\mathbf{w}^t$ and $\mathbf{v}^t$ are mutually independent white Gaussian noise processes such that: $E\{\mathbf{w}^t(k)\mathbf{w}^t(l)\} = \mathbf{Q}_d^t(k)\delta_{kl}$ and $E\{\mathbf{v}^t(k)\mathbf{v}^t(l)\} = \mathbf{R}^t(k)\delta_{kl}$. If the initial PDF of the target state is Gaussian, then the standard Kalman filter can be used for system propagation and measurement updates. Note that the assumption of linearity can be relaxed, and the Kalman filter could be replaced with an extended Kalman filter.[6] In the development that follows, time indices have been removed from system matrices for convenience. Applying Bayes' rule to the joint target state PDF gives:

$$\begin{aligned} f\{\mathbf{X}(k)|\mathbf{Z}^k\} &= f\{\mathbf{X}(k)|\mathbf{Z}(k), \mathbf{Z}^{k-1}, N_m(k)\} \\ &= \frac{f\{\mathbf{X}(k), \mathbf{Z}(k)|\mathbf{Z}^{k-1}, N_m(k)\}}{f\{\mathbf{Z}(k)|\mathbf{Z}^{k-1}, N_m(k)\}} \\ &= \frac{f\{\mathbf{Z}(k)|\mathbf{X}(k), \mathbf{Z}^{k-1}, N_m(k)\} f\{\mathbf{X}(k)|\mathbf{Z}^{k-1}, N_m(k)\}}{f\{\mathbf{Z}(k)|\mathbf{Z}^{k-1}, N_m(k)\}} \\ &= \frac{f\{\mathbf{Z}(k)|\mathbf{X}(k), N_m(k)\} f\{\mathbf{X}(k)|\mathbf{Z}^{k-1}\}}{f\{\mathbf{Z}(k)|\mathbf{Z}^{k-1}, N_m(k)\}} \end{aligned} \tag{3}$$

where $N_m(k)$ is the number of measurements in the combined gating region at time $k$, which is inherent in the knowledge of the measurements themselves. Notice that the last step removes dependence on $\mathbf{Z}^{k-1}$ in the first numerator term since the current measurements are assumed independent of the measurement history. Also, dependence on $N_m(k)$ can be removed from the second numerator term since the joint state is independent of the number of measurements. Define $\Theta_l(k)$ as a joint association hypothesis in which each target $t$ out of T targets is associated with an individual measurement $\mathbf{z}_{l_t}$ from a set of $N_m$ measurements within the combined gate of the targets within a cluster. This can be expressed as the set of individual target hypothesis $\theta_{l_t}^t(k)$ in which target $t$ is associated with measurement $l_t$ and where $l_t = 0$ indicates that the target is not detected. The time index will be dropped for convenience.

$$\Theta_l(k) = \{\theta_{l_1}^1, \theta_{l_2}^2, ..., \theta_{l_\mathrm{T}}^\mathrm{T}\} \tag{4}$$

The first term of the numerator of Eq. (3) can be expressed as:

$$f\{\mathbf{Z}(k)|\mathbf{X}(k), N_m(k)\} = \sum_l f\{\mathbf{Z}(k)|\mathbf{X}(k), \Theta_l(k), N_m(k)\} P\{\Theta_l(k)|\mathbf{X}(k), N_m(k)\} \tag{5}$$

When considering individual measurements $\mathbf{z}_{l_t}$ associated with target $t$, the first term in Eq. (5) can be written as:

$$f\{\mathbf{Z}(k)|\mathbf{X}(k),\Theta_l(k),N_m(k)\} = \prod_{\xi=1}^{N_m(k)} f\{\mathbf{z}_\xi(k)|\mathbf{x}^{t(\Theta_l(k),\xi)}(k),\Theta_l(k),N_m(k)\} \tag{6}$$

given that we assume independence of the measurements conditioned on an association event, and where $t(\Theta_l(k),\xi)$ is the index of the target associated with measurement $\xi$ under the joint association event $\Theta_l(k)$ (or zero if the measurement is not associated with a target under the event). Since the density is conditioned on the true state and we know $\mathbf{z}_\xi(k) = \mathbf{H}\mathbf{x}^{t(\Theta_l(k),\xi)}(k) + \mathbf{v}^{t(\Theta_l(k),\xi)}(k)$, we get:

$$f\{\mathbf{z}_\xi(k)|\mathbf{x}^t(k),\Theta_l(k),N_m(k)\} = \begin{cases} \mathcal{N}\{\mathbf{z}_\xi(k);\mathbf{H}\mathbf{x}^{t(\Theta_l(k),\xi)}(k),\mathbf{R}^{t(\Theta_l(k),\xi)}\} & ,t(\Theta_l(k),\xi)>0 \\ V^{-1} & ,t(\Theta_l(k),\xi)=0 \end{cases} \tag{7}$$

where $V$ is the hypervolume of the region defined by the measurement gates of all the targets within a cluster.[7] The second term in Eq. (5):

$$P\{\Theta_l(k)|\mathbf{X}(k),N_m(k)\} = P\{\Theta_l(k)|N_m(k)\} \tag{8}$$

is shown[7] to be:

$$P\{\Theta_l(k)|\mathbf{X}(k),N_m(k)\} = \frac{(\lambda V)^\phi e^{-\lambda V}}{N_m!} P_{dg}^\psi (1-P_{dg})^{\mathrm{T}-\psi} = \frac{1}{c_1}(\lambda V)^\phi P_{dg}^\psi (1-P_{dg})^{\mathrm{T}-\psi} \tag{9}$$

where $\lambda$ is the clutter density (the expected number of clutter measurements per unit volume within the gated region), $P_{dg}$ is the probability that any one target within the cluster will be detected and the resulting measurement is within the gate, $\phi$ is the number of measurements originating from clutter, and $\psi$ is the number of detected targets ($\phi+\psi=N_m$). Note that if $P_d$ is the target detection probability and $P_g$ is the probability that the target-oriented measurement is within the association gate, then $P_{dg} = P_d P_g$. In the derivation of Eq. (9), a Poisson distribution for the clutter model is assumed such that:

$$P\{\phi\} = \frac{(\lambda V)^\phi e^{-\lambda V}}{\phi!} \tag{10}$$

When forming the product of Eq. (6) and Eq. (9) we see Eq. (6) will include a $V^{-1}$ term for each measurement believed to be the result of clutter, of which there will be $\phi$, and Eq. (9) contains a $V^\phi$ term, so these terms will cancel. Also, the constant $c_1$ becomes part of a normalization constant when summing over all the association events. Since targets within a cluster cannot share the same measurement, it is convenient to define a flag:

$$F(\Theta_l(k)) = F(\theta_{l_1}^1,\theta_{l_2}^2,...,\theta_{l_\mathrm{T}}^\mathrm{T}) = \begin{cases} 1 & ,\text{ no shared measurement} \\ 0 & ,\text{ shared measurement} \end{cases} \tag{11}$$

that when combined with the product of Eq. (6) and Eq. (9) will preclude targets from sharing the same measurement. In effect, $F(\Theta_l(k))$ is a flag indicating whether an association event is consistent. Given that target $t$ is associated with measurement $l_t$, the final expression for Eq. (5) by substituting Eq. (7) into Eq. (6) then combining with Eq. (9) becomes:

$$f\{\mathbf{Z}(k)|\mathbf{X}(k),N_m(k)\} = \sum_{l_1=0}^{N_m(k)} \sum_{l_2=0}^{N_m(k)} \cdots \sum_{l_T=0}^{N_m(k)} \mathrm{M}_{l_1}^1 \mathrm{M}_{l_2}^2 ... \mathrm{M}_{l_\mathrm{T}}^\mathrm{T} \cdot F(\theta_{l_1}^1,\theta_{l_2}^2,...,\theta_{l_\mathrm{T}}^\mathrm{T}) \cdot \frac{1}{c_1} \tag{12}$$

given the following definition:

$$\mathrm{M}_{l_t}^t = \begin{cases} \mathcal{N}\{\mathbf{z}_{l_t}(k);\mathbf{H}\mathbf{x}^t(k),\mathbf{R}^t\}P_{dg} & l_t>0 \\ \lambda(1-P_{dg}) & l_t=0 \end{cases}$$

Note that $l_t=0$ represents the case when target $t$ is associated with clutter and thus $\mathrm{M}_0^t = \lambda(1-P_{dg})$ given the cancellation of the $V^{-1}$ terms discussed previously. The summation of all $l$ joint hypotheses is represented by the nested sums of the individual target hypotheses.

The second term of the numerator of Eq. (3) is the joint target state PDF from the prior sample period and can be expressed as:

$$f\{\mathbf{X}(k)|\mathbf{Z}^{k-1}\} = \sum_j f\{\mathbf{X}(k)|\mathbf{Z}^{k-1}, \Theta_j^{k-1}\} P\{\Theta_j^{k-1}|\mathbf{Z}^{k-1}\} \tag{13}$$

where $\Theta_j^{k-1} = \{\Theta(1), \Theta(2), ...\Theta(k-1)\}$ represents the joint association history hypotheses from the prior sample period. If we assume independence between targets conditioned on a given hypothesis, then:

$$f\{\mathbf{X}(k)|\mathbf{Z}^{k-1}, \Theta_j^{k-1}\} = \prod_{t=1}^{\mathrm{T}} f\{\mathbf{x}^t(k)|\mathbf{Z}^{k-1}, \Theta_j^{k-1}\} \tag{14}$$

where the individual PDF's are represented as a Gaussian given by:

$$\mathrm{N}_{j_t}^t = f\{\mathbf{x}^t(k)|\mathbf{Z}^{k-1}, \Theta_j^{k-1}\} = \mathcal{N}\{\mathbf{x}^t(k); \boldsymbol{\mu}_{j_t}^t(k^-), \mathbf{P}_{j_t}^t(k^-)\} \tag{15}$$

where $\boldsymbol{\mu}_{j_t}^t(k^-)$ and $\mathbf{P}_{j_t}^t(k^-)$ are the mean and covariance of target $t$ based on the single target hypothesis $j_t$ at time $k$ prior to a measurement update. Also, $P\{\Theta_j^{k-1}|\mathbf{Z}^{k-1}\}$ is the joint hypothesis probability from the previous sample period and can be represented as T-dimensional array, $P_{j_1 j_2 ... j_\mathrm{T}}(k-1)$. Eq. (13) can now be represented as nested summations of the single target hypotheses:

$$f\{\mathbf{X}(k)|\mathbf{Z}^{k-1}\} = \sum_{j_1=1}^{N_{h_1}(k-1)} \sum_{j_2=1}^{N_{h_2}(k-1)} \cdots \sum_{j_\mathrm{T}=1}^{N_{h_\mathrm{T}}(k-1)} \mathrm{N}_{j_1}^1 \mathrm{N}_{j_2}^2 ... \mathrm{N}_{j_\mathrm{T}}^\mathrm{T} P_{j_1 j_2 ... j_\mathrm{T}}(k-1) \tag{16}$$

where $N_{h_t}(k-1)$ is the number of single target hypotheses for target $t$ at time $k-1$.

Finally, forming the overall numerator of Eq. (3) results in:

$$\begin{aligned} f\{\mathbf{X}(k)|\mathbf{Z}^k\} &= \frac{1}{c_2} \sum_{l_1=0}^{N_m(k)} \sum_{l_2=0}^{N_m(k)} \cdots \sum_{l_T=0}^{N_m(k)} \mathrm{M}_{l_1}^1 \mathrm{M}_{l_2}^2 ... \mathrm{M}_{l_\mathrm{T}}^\mathrm{T} \cdot F(\theta_{l_1}^1, \theta_{l_2}^2, ..., \theta_{l_\mathrm{T}}^\mathrm{T}) \\ &\quad \sum_{j_1=1}^{N_{h_1}(k-1)} \sum_{j_2=1}^{N_{h_2}(k-1)} \cdots \sum_{j_\mathrm{T}=1}^{N_{h_\mathrm{T}}(k-1)} \mathrm{N}_{j_1}^1 \mathrm{N}_{j_2}^2 ... \mathrm{N}_{j_\mathrm{T}}^\mathrm{T} P_{j_1 j_2 ... j_\mathrm{T}}(k-1) \end{aligned} \tag{17}$$

where $c_2$ is a normalization value formed by the denominator of Eq. (3) and the constant $c_1$ in Eq. (9) such that the sum of all the joint association events and hence the integral of the density in Eq. (17) is one. Changing the order of summation gives:

$$\begin{aligned} f\{\mathbf{X}(k)|\mathbf{Z}^k\} &= \frac{1}{c_2} \sum_{l_1=0}^{N_m(k)} \sum_{j_1=1}^{N_{h_1}(k-1)} \sum_{l_2=0}^{N_m(k)} \sum_{j_2=1}^{N_{h_2}(k-1)} \cdots \sum_{l_T=0}^{N_m(k)} \sum_{j_\mathrm{T}=1}^{N_{h_\mathrm{T}}(k-1)} \left(\mathrm{N}_{j_1}^1 \mathrm{M}_{l_1}^1\right) \left(\mathrm{N}_{j_2}^2 \mathrm{M}_{l_2}^2\right) ... \left(\mathrm{N}_{j_\mathrm{T}}^\mathrm{T} \mathrm{M}_{l_\mathrm{T}}^\mathrm{T}\right) \bullet \\ &\quad F(\theta_{l_1}^1, \theta_{l_2}^2, ..., \theta_{l_\mathrm{T}}^\mathrm{T}) P_{j_1 j_2 ... j_\mathrm{T}}(k-1) \end{aligned} \tag{18}$$

and considering the $\mathrm{N}_{j_t}^t$ and $\mathrm{M}_{l_t}^t$ terms alone allows incorporation of the Kalman measurement update in a manner synonymous with the development in Maybeck[8]:

$$\begin{aligned} \mathrm{N}_{j_t}^t \mathrm{M}_{l_t}^t &= \mathcal{N}\{\mathbf{x}^t(k); \boldsymbol{\mu}_{j_t}^t(k^-), \mathbf{P}_{j_t}^t(k^-)\} \mathcal{N}\{\mathbf{z}_{l_t}(k); \mathbf{H}\mathbf{x}^t(k), \mathbf{R}^t\} P_{dg} && , l_t > 0 \\ &= \mathcal{N}\{\mathbf{x}^t(k); \boldsymbol{\mu}_{j_t}^t(k^+), \mathbf{P}_{j_t}^t(k^+)\} \mathcal{N}\{\mathbf{z}_{l_t}(k); \mathbf{H}\boldsymbol{\mu}_{j_t}^t(k^-), \mathbf{H}\mathbf{P}_{j_t}^t(k^-)\mathbf{H}^{'} + \mathbf{R}^t\} P_{dg} && , l_t > 0 \end{aligned} \tag{19}$$

where:

$$\begin{aligned} \boldsymbol{\mu}_{j_t}^t(k^+) &= \boldsymbol{\mu}_{j_t}^t(k^-) + \mathbf{K}_{j_t}^t(k)[\mathbf{z}_{l_t}(k) - \mathbf{H}\boldsymbol{\mu}_{j_t}^t(k^-)] \\ \mathbf{P}_{j_t}^t(k^+) &= \mathbf{P}_{j_t}^t(k^-) - \mathbf{K}_{j_t}^t(k)\,\mathbf{H}\mathbf{P}_{j_t}^t(k^-) \\ \mathbf{K}_{j_t}^t(k) &= \mathbf{P}_{j_t}^t(k^-)\mathbf{H}^T(\mathbf{H}\mathbf{P}_{j_t}^t(k^-)\mathbf{H}^{'} + \mathbf{R}^t)^{-1} \end{aligned} \tag{20}$$

For simplicity, based on Eq. (19) define:

$$\begin{aligned} \mathrm{U}^t_{l_t j_t} &= \mathcal{N}\{\mathbf{x}^t(k); \boldsymbol{\mu}^t_{j_t}(k^+), \mathbf{P}^t_{j_t}(k^+)\} \\ \mathrm{W}^t_{l_t j_t} &= \mathcal{N}\{\mathbf{z}_{l_t}(k); \mathbf{H}\boldsymbol{\mu}^t_{j_t}(k^-), \mathbf{H}\mathbf{P}^t_{j_t}(k^-)\mathbf{H}^{'} + \mathbf{R}^t\} P_{dg} \ , l_t > 0 \end{aligned}$$

Note that for $l_t = 0$, $M^t_{l_t} = \lambda(1 - P_{dg}) \Rightarrow W^t_{l_t j_t} = \lambda(1 - P_{dg}) \Rightarrow U^t_{l_t j_t} = N^t_{j_t}$. Rewriting Eq. (18), incorporating the measurement update and combining the double sums over $l_t$ and $j_t$ into a single sum over $i_t$ with a new upper limit given by $N_{h_t}(k) = N_{h_t}(k-1)(N_m(k)+1)$ gives:

$$\begin{aligned} f\{\mathbf{X}(k)|\mathbf{Z}^k\} &= \frac{1}{c_2} \sum_{i_1=1}^{N_{h_1}(k)} \sum_{i_2=1}^{N_{h_2}(k)} \cdots \sum_{i_T=1}^{N_{h_\mathrm{T}}(k)} \left(\mathrm{U}^1_{i_1} \mathrm{W}^1_{i_1}\right) \left(\mathrm{U}^2_{i_2} \mathrm{W}^2_{i_2}\right) ... \left(\mathrm{U}^\mathrm{T}_{i_\mathrm{T}} \mathrm{W}^\mathrm{T}_{i_\mathrm{T}}\right) \bullet \\ & \quad F(\theta^1_{l_1(i_1)}, \theta^2_{l_2(i_2)}, ..., \theta^\mathrm{T}_{l_\mathrm{T}(i_\mathrm{T})}) P_{j_1(i_1) j_2(i_2) ... j_\mathrm{T}(i_\mathrm{T})}(k-1) \end{aligned} \tag{21}$$

where the indexing is simplified as $\mathrm{U}^t_{l_t j_t} = \mathrm{U}^t_{i_t}$ and similarly for W. From an implementation standpoint, the joint target state PDF shown in Eq. (18) is maintained in two parts. First, when calculating the single target hypotheses, the updated parameters $\mathrm{U}^t_{i_t}$ are computed. Second, the joint hypothesis probability array at time $k$ is calculated via:

$$P_{i_1 i_2 ... i_\mathrm{T}}(k) = \frac{1}{c_3} \left(\mathrm{W}^1_{i_1} \mathrm{W}^2_{i_2} ... \mathrm{W}^\mathrm{T}_{i_\mathrm{T}}\right) F(\theta^1_{l_1(i_1)}, \theta^2_{l_2(i_2)}, ..., \theta^\mathrm{T}_{l_\mathrm{T}(i_\mathrm{T})}) P_{j_1(i_1) j_2(i_2) ... j_\mathrm{T}(i_\mathrm{T})}(k-1) \tag{22}$$

where $c_3$ is a normalization constant such that the terms in $P_{i_1 i_2 ... i_\mathrm{T}}(k)$ sum to unity. Note that the new dimension of the joint hypothesis probability array at time $k$ would potentially be:

$$[N_{h_1}(k-1)(N_m(k)+1) \text{ x } N_{h_2}(k-1)(N_m(k)+1) \text{ x...x } N_{h_\mathrm{T}}(k-1)(N_m(k)+1)] \tag{23}$$

Since gating will preclude many of the rows (hyper-rows with more than two dimensions) from being necessary, the actual dimensions will tend to be smaller. However, the number of hypotheses grows exponentially with time and with the number of targets, emphasizing the need for some method of hypothesis reduction.

Given the updated joint hypothesis probability in Eq. (22) at time $k$ an updated marginal probability for each single target hypothesis at time $k$ can be found by marginalizing the joint target PDF $f\{\mathbf{X}(k)|\mathbf{Z}^k\}$. Specifically,

$$\begin{aligned} f\{\mathbf{x}^1(k)|\mathbf{Z}^k\} &= \int \cdots \int f\{\mathbf{X}(k)|\mathbf{Z}^k\} d\mathbf{x}^2 ... d\mathbf{x}^\mathrm{T} \\ &= \int \cdots \int \left[ \sum_{j_1=1}^{N_{h_1}(k)} \sum_{j_2=1}^{N_{h_2}(k)} \cdots \sum_{j_\mathrm{T}=1}^{N_{h_\mathrm{T}}(k)} \mathrm{N}^1_{j_1} \mathrm{N}^2_{j_2} ... \mathrm{N}^\mathrm{T}_{j_\mathrm{T}} P_{j_1 j_2 ... j_\mathrm{T}}(k) \right] d\mathbf{x}^2 ... d\mathbf{x}^\mathrm{T} \\ &= \sum_{j_1=1}^{N_{h_1}(k)} \left[ \sum_{j_2=1}^{N_{h_2}(k)} \cdots \sum_{j_\mathrm{T}=1}^{N_{h_\mathrm{T}}(k)} P_{j_1 j_2 ... j_\mathrm{T}}(k) \right] \mathrm{N}^1_{j_1} \int \mathrm{N}^2_{j_2} d\mathbf{x}^2 \cdots \int \mathrm{N}^\mathrm{T}_{j_\mathrm{T}} d\mathbf{x}^\mathrm{T} \\ &= \sum_{j_1=1}^{N_{h_1}(k)} \mathrm{J}^1_{j_1} \mathrm{N}^1_{j_1} \end{aligned} \tag{24}$$

where $\mathrm{J}^1_{j_1} = \sum_{j_2=1}^{N_{h_2}(k)} \cdots \sum_{j_\mathrm{T}=1}^{N_{h_\mathrm{T}}(k)} P_{j_1 j_2 ... j_\mathrm{T}}(k)$ is the marginal hypothesis probability for target 1. Clearly, $\mathrm{J}^t_{j_t}$ can be calculated for any target by simply summing the joint hypothesis probability array over all its dimensions except for the one associated with target $t$. Eq. (24) clearly illustrates the difference between the joint and marginal hypothesis probabilities, the former providing information about the correlation between targets while the later gives the probability weight for each single target hypothesis. For illustration purposes, consider the two-target example shown in Figure 1 where it is assumed that each target had only a single association hypothesis from the previous processing cycle. The joint probability array prior to normalization is shown in Table 1 and is calculated using Eq. (22) where the marginal hypothesis probabilities are calculated by summing over the columns for target $t_1$ and the rows for target $t_2$. At this point, the probability weights are available for use in calculating the combined state estimate and covariance and to reduce the Gaussian mixture representing the joint target state PDF.

| | | $t_2$ | | | | | |
|---|---|---|---|---|---|---|---|
| | $P_{j_1 j_2}$ | $m_0$ | $m_1$ | $m_2$ | $m_3$ | | |
| | $m_0$ | $\mathrm{W}_0^1\mathrm{W}_0^2$ | $\mathrm{W}_0^1\mathrm{W}_1^2$ | $\mathrm{W}_0^1\mathrm{W}_2^2$ | $\mathrm{W}_0^1\mathrm{W}_3^2$ | $\rightarrow$ | $\mathrm{J}_1^1$ |
| $t_1$ | $m_1$ | $\mathrm{W}_1^1\mathrm{W}_0^2$ | 0 | $\mathrm{W}_1^1\mathrm{W}_2^2$ | $\mathrm{W}_1^1\mathrm{W}_3^2$ | $\rightarrow$ | $\mathrm{J}_2^1$ |
| | $m_2$ | $\mathrm{W}_2^1\mathrm{W}_0^2$ | $\mathrm{W}_2^1\mathrm{W}_1^2$ | 0 | $\mathrm{W}_2^1\mathrm{W}_3^2$ | $\rightarrow$ | $\mathrm{J}_3^1$ |
| | | $\downarrow$ | $\downarrow$ | $\downarrow$ | $\downarrow$ | | |
| | | $\mathrm{J}_1^2$ | $\mathrm{J}_2^2$ | $\mathrm{J}_3^2$ | $\mathrm{J}_4^2$ | | |

**Table 1.** Joint probability array: two-target example. The rows represent the different associations for target 1, while the columns represent the associations for target 2. Association with measurement $m_0$ denotes that detection of the target was missed.

### 2.2. ISE reduction

The ISE hypothesis reduction method[1,2] is based on a cost function which directly measures the difference or similarity between the original PDF and potential reduced order approximations of this PDF. Define the original PDF as $f\{\mathbf{x}^t(k)|\Omega_{N_{h_t}}(k)\}$, where $\Omega_{N_{h_t}}(k)$ represents the parameters of the $N_{h_t}(k)$ hypotheses for target $t$ derived from the measurements up to the current sample period. The goal is to reduce these $N_{h_t}(k)$ hypotheses to a simplified representation, containing $N_{r_t}(k)$ hypotheses (the subscript 'r' denoting 'reduced'), resulting in the simplified PDF, $f\{\mathbf{x}^t(k)|\Omega_{N_{r_t}}(k)\}$. The cost function value is used to evaluate whether one PDF approximation is "better" than another, with a goal of minimizing the Integral Square Error cost given by:

$$J = \int (f\{\mathbf{x}^t(k)|\Omega_{N_{h_t}}(k)\} - f\{\mathbf{x}^t(k)|\Omega_{N_{r_t}}(k)\})^2 d\mathbf{x}^t(k) \tag{25}$$

For the MHT structure presented in this paper, the PDF used in the ISE reduction is the marginalized target state PDF, $f\{\mathbf{x}^t(k)|\mathbf{Z}^k\}$ given by Eq. (24). The ISE algorithm utilizes Eq. (25) to determine merging and pruning actions to be performed on the Gaussian mixture components which will tend to produce a small increase in the ISE cost function. The possible actions are to delete one of the remaining components, or to merge a pair of components. When two components are merged, the parameters of the merged component are calculated such that the mean and covariance of the overall mixture remains unchanged.[1] Based on the decisions dictated by the ISE reduction method, it is necessary to update the joint hypothesis probability array and the associated marginal probabilities. In the event of a hypothesis deletion, the corresponding elements of the joint array are removed. Hypothesis merging results in summing elements of the joint array corresponding to the hypotheses being merged. Referring again to the two-target example of Table 1, merging hypothesis associated with measurements $m_1$ and $m_2$ for target 2 would result in adding the respective columns of the joint array.

## 3. RESULTS AND ANALYSIS

### 3.1. Scenario Definition

Performance characteristics were determined via Monte Carlo simulations on various two-target scenarios. For each target, the dynamics and measurement models were identical and time-invariant for simplicity. Specifically, let the state vector $\mathbf{x}^t = [x\ \dot{x}\ y\ \dot{y}]'$ represent the target's position and velocity with:

$$\mathbf{\Phi}^t = \begin{bmatrix} 1 & T_s & 0 & 0 \\ 0 & 1 & 0 & 0 \\ 0 & 0 & 1 & T_s \\ 0 & 0 & 0 & 1 \end{bmatrix}, \qquad \mathbf{G}_d^t = \begin{bmatrix} \frac{T_s^2}{2} & 0 \\ T_s & 0 \\ 0 & \frac{T_s^2}{2} \\ 0 & T_s \end{bmatrix}, \qquad \mathbf{Q}_d^t = \begin{bmatrix} q_x & 0 \\ 0 & q_y \end{bmatrix}$$

$$\mathbf{H} = \begin{bmatrix} 1 & 0 & 0 & 0 \\ 0 & 0 & 1 & 0 \end{bmatrix}, \qquad \mathbf{R} = \begin{bmatrix} r & 0 \\ 0 & r \end{bmatrix}$$

In all cases, data was collected over 100 Monte Carlo runs and 30 time steps per run. The following parameter values remained unchanged for all of the scenarios: $\lambda = 0.012$, $P_d = 1$, $P_g = 0.99$, $r = 1$, and $T_s = 1$, where

| | Target 1 | | | | Target 2 | | | |
|---|---|---|---|---|---|---|---|---|
| Scenario | $x^1$ | $\dot{x}^1$ | $y^1$ | $\dot{y}^1$ | $x^2$ | $\dot{x}^2$ | $y^2$ | $\dot{y}^2$ |
| 1 | 0 | 0 | 0 | 5 | 3 | 0 | 0 | 5 |
| 2 | 0 | 0 | 0 | 5 | 6 | 0 | 0 | 5 |
| 3 | 0 | 0.2 | 0 | 1 | 6 | -0.2 | 0 | 1 |
| 4 | 0 | 10 | 0 | 10 | 200 | -10 | 0 | 10 |

**Table 2.** Initial parameter values for scenarios

$T_s$ is the time between measurement intervals $(k-1)$ to $k$. Table 2 shows the various initial conditions chosen for each scenario. Since a constant velocity model was simulated, the initial values for the velocities dictate the trajectory of the targets corrupted by dynamics noise. Low dynamics noise for the truth model ($q_x = q_y = 0.001$) and high dynamics noise ($q_x = q_y = 1$) cases were generated. Scenario 1 represents two closely space targets travelling in formation. At each sample time, the random dynamics noise generated for the truth model was the same for both targets in each axis to ensure target formation would be maintained (i.e., the noise processes were perfectly coupled). Scenario 2 is the same as scenario 1, except the target spacing is slightly increased. Scenario 3 represents two slowly crossing targets, increasing the potential for track coalescence. Scenario 4 initializes the targets locations far apart and the velocities ensure that the targets cross relatively quickly. It is important to note that in keeping the randomly generated dynamics noise for both targets the same and thus inducing the physically meaningful case of formation flight, we have induced a significant amount of correlation when compared to the case where the two targets had independent dynamic noise samples. The effects of this will be discussed further in Section 3.4.

### 3.2. Combined estimate

A combined state estimate for the each track is initially computed as a weighted sum of the single target hypothesis given by:

$$\hat{\mathbf{x}}^t(k) = \sum_{j_t=1}^{N_{h_t}(k)} \mathrm{J}^t_{j_t}(k)\boldsymbol{\mu}^t_{j_t}(k) \tag{26}$$

When targets are closely spaced it is common for a track on one target to begin tracking a neighboring target thus losing track continuity. This can result in a track swapping between targets, or track coalescence can occur (track coalescence refers to the case when two or more tracks converge to a mid-point between targets and effectively coalesce into one track). The underlying cause of these problems is identified when viewing the behavior of the single target hypotheses which tend to defect away from their original target and gravitate towards a neighboring target. In order to mitigate hypothesis defection and ultimately mitigate track coalescence or swapping, a method needs to be employed which eliminates the defecting hypothesis from the calculation of the final combined state estimate. A simplistic *ad hoc* approach is to first generate initial combined estimates for each track via Eq. (26), then compute the distance or squared error from each single target hypothesis estimate to each of the initial combined estimates. This distance is typically in Euclidean space, such that only those states representing the target position are used in the calculation. Other distance measures may prove more appropriate for other applications. If a single target hypothesis for a given target is closer to the combined estimate for another target than to the combined estimate for the target to which it belongs, then this hypothesis is said to defect. This is expressed as:

$$\left\|\boldsymbol{\mu}^t_{j_t}(k) - \hat{\mathbf{x}}^t(k)\right\| > \left\|\boldsymbol{\mu}^t_{j_t}(k) - \hat{\mathbf{x}}^{\tilde{t}}(k)\right\| \text{ for } t \neq \tilde{t} \Rightarrow \text{hypothesis defecting} \tag{27}$$

The final combined estimate is then calculated using Eq. (26) with only those hypotheses that have not been identified as defecting and then normalized appropriately. Similarly, the combined covariance is calculated via:

$$\mathbf{P}^t(k) = \sum_{j_t=1}^{N_{h_t}(k)} \mathrm{J}^t_{j_t}(k)\left\{\mathbf{P}^t_{j_t}(k) + \left[\hat{\mathbf{x}}^t(k) - \boldsymbol{\mu}^t_{j_t}(k)\right]\left[\hat{\mathbf{x}}^t(k) - \boldsymbol{\mu}^t_{j_t}(k)\right]'\right\} \tag{28}$$

using only the non-defecting hypotheses and again normalizing appropriately. Alternatively, one could delete the defecting hypotheses from the set of single target hypotheses, updating the joint hypothesis probability array by deleting the appropriate entries and re-normalizing. The marginal probabilities, $\mathrm{J}^t_{j_t}$, are also re-normalized, and a final combined estimate is calculated using Eq. (26) with the reduced set of single target hypothesis. In the two-target example, deleting a hypothesis would result in deleting the appropriate row in the joint hypothesis array for target 1 or the appropriate column for target 2. This approach makes hard decisions about hypothesis pruning, which will tend to skew the mean estimates away from each other.

### 3.3. Identification measurements

Although the primary source of measurement data was assumed to be a radar type system, providing anonymous unlabeled position-type data, an identification type of measurement such as IFF was included in order to *exploit* the potential benefits of incorporating the joint state correlation information. The concept was when the targets are well separated the tracks can easily avoid the ambiguity of which target they are tracking; however, when the targets become closely spaced, this ambiguity arises and track swap may readily occur. Maintaining correlation information allows us to recognize that there are two targets in one of two estimated positions (e.g., target 1 in position A and target 2 in position B OR target 1 in position B and target 2 in position A); we do not know which of these two cases is true. However, if we later learn via IFF data that target 1 is in position B, then with correlation information we know position A applies to target 2. The ability to perfectly match the identification measurement to the correct target is unrealistic and in practice some form of probabilistic method would be implemented to account for the inherent uncertainty in the IFF data. However, the ideal approach was implemented to test the potential benefit of target attribute measurements within the construct of correlation exploitation.

A very simple model was employed that provided position data in one axis and at a slower sampling rate (arbitrarily set at 12 time steps) than the primary radar data. The intent of this IFF type measurement was not to improve the quality of the state estimate for position, but to resolve track to target ambiguity through the implicit modification of the hypothesis association probabilities. The IFF type model is as follows:

$$\begin{aligned} z_{\text{iff}} &= \mathbf{H}_{\text{iff}}\mathbf{x}^t + v_{\text{iff}} \\ \mathbf{H}_{\text{iff}} &= \begin{bmatrix} 1 & 0 & 0 & 0 \end{bmatrix} \qquad R_{\text{iff}} = 1 \end{aligned} \tag{29}$$

Since the IFF data includes the target ID, this measurement is only applied to the target with this unique ID. In the scenarios, IFF measurements were generated only for target 1. Since the IFF measurement inherently indicates which target is associated with the measurement data, a Kalman update will only be applied to those hypotheses associated with this target. Specifically, the mean and covariance will be updated using Eq. (20) based on system matrices $\mathbf{H}_{\text{iff}}$ and $R_{\text{iff}}$ for a single target $t$. The probability will be modified based on the joint state PDF:

$$f\{\mathbf{X}(k)|\mathbf{Z}^k, z_{\text{iff}}\} = \frac{f\{z_{\text{iff}}(k)|\mathbf{X}(k)\}f\{\mathbf{X}(k)|\mathbf{Z}^k\}}{f\{z_{\text{iff}}(k)|\mathbf{Z}^k\}} \propto f\{z_{\text{iff}}(k)|\mathbf{X}(k)\}f\{\mathbf{X}(k)|\mathbf{Z}^k\} \tag{30}$$

Based on the same development shown via Eqs. (17) - (20), the means and covariances for the target associated with the IFF measurement are updated via the Kalman update equations. Furthermore, if the joint target correlation is maintained via the joint probability array, then Eq. (30) results in the multiplication of:

$$f\{z_{\text{iff}}(k)|\mathbf{Z}^k_{j_t}\} = \mathcal{N}\{z_{\text{iff}}(k); \mathbf{H}_{\text{iff}}\boldsymbol{\mu}^t_{j_t}(k), \mathbf{H}_{\text{iff}}\mathbf{P}^t_{j_t}(k)\mathbf{H}^{'}_{\text{iff}} + R_{\text{iff}}\} \tag{31}$$

and each element of Eq. (22) related to the IFF associated target followed by re-normalization. Referring to the two-target example and assuming the IFF measurement is associated with target $t_1$, each row of the array would be multiplied by Eq. (31) based on the appropriate values of $\boldsymbol{\mu}^t_{j_t}$ and $\mathbf{P}^t_{j_t}$, then re-normalized. The marginal hypothesis probabilities are recomputed according to Eq. (24). Alternatively, if correlation is *not* maintained, then $f\{\mathbf{X}(k)|\mathbf{Z}^k\}$ is represented by the marginalized PDF of Eq. (24). The Bayesian probability update then becomes:

$$\mathrm{J}^t_{j_t}(k^+) = f\{z_{\text{iff}}(k)|\mathbf{Z}^k_{j_t}\}\mathrm{J}^t_{j_t}(k^-) \tag{32}$$

The measurement is also used to perform a Kalman update via Eq. (20) on the parameter of the single-target hypotheses for the appropriate target.

### 3.4. Analysis

Performance evaluation is based on the following metrics: track swap, track coalescence, track life, and RMS position error. A more general form of track swap is the lack of track continuity as defined in Blackman.[9] For the two-target scenarios presented here, track swap is declared when the combined estimates (tracks) for each target swap and begin tracking the other target. This is determined when:

$$\left|\mathbf{H}\hat{\mathbf{x}}^{t}(k) - \mathbf{H}\mathbf{x}^{t}(k)\right| > \left|\mathbf{H}\hat{\mathbf{x}}^{t}(k) - \mathbf{H}\mathbf{x}^{\tilde{t}}(k)\right| \text{ for } t \neq \tilde{t} \tag{33}$$

indicating that the combined estimate for target $t$ has swapped to target $\tilde{t}$. Since tracks may swap back and forth throughout a given sequence of measurements and in some cases resolve themselves back to their original target, a complete swap is only declared if both tracks are swapped at the terminal time in the simulation. Based on a useful measure presented by Blom and Bloem,[10] two tracks, $t \neq \tilde{t}$, are considered coalesced at time $k$ if:

$$\left|\mathbf{H}\hat{\mathbf{x}}^{t}(k) - \mathbf{H}\hat{\mathbf{x}}^{\tilde{t}}(k)\right| \leq \sigma_{sep} \cap \left|\mathbf{H}\mathbf{x}^{t}(k) - \mathbf{H}\mathbf{x}^{\tilde{t}}(k)\right| > \sigma_{sep} \tag{34}$$

where $\sigma_{sep}$ indicates the minimum separation allowed between tracks before coalescence is considered. Note that $\sigma_{sep} = 1.5$ based on empirical analysis for the given scenarios. Track life indicates the length of time that a target was tracked prior to track loss. A measure of track life[11] formed the basis of the track loss metric:

$$\left[\hat{\mathbf{x}}^{t}(k) - \mathbf{x}^{t}(k)\right]^{T} \mathbf{P}_{p}^{-1} \left[\hat{\mathbf{x}}^{t}(k) - \mathbf{x}^{t}(k)\right] > 10 \tag{35}$$

where $\mathbf{P}_p$ represents the covariance of a Kalman filter without association uncertainty. Blackman[9] suggests using the filtered track covariance $\mathbf{P}^t$. However, in cases where the association uncertainty of the track has grown relatively large, the overall quadratic in Eq. (35) may be inappropriately reduced by the $\mathbf{P}^{t^{-1}}$ term when comparisons to the true target state are concerned. In the two-target scenarios, a track loss was declared when Eq. (35) was satisfied for either track for 5 consecutive time steps. Since track swap may occur at any time, Eq. (35) was computed for each track/target pair and the minimum value was compared to the empirically determined threshold.

Table 3 shows the percentage of run time when tracks coalesced for each scenario. The algorithms implemented include:

- ISE_C_D - MISER with correlation and management of hypothesis defection as defined in Section 3.2
- ISE_C - MISER with correlation only and hypothesis defection was not mitigated

with 10 mixture reduction components in both cases. In all cases when track coalescence occurred, it was reduced when the management of hypothesis defection was implemented. In most cases, this reduction is very significant indicating the need for some method of managing the defections. Figure 2 illustrates a single run example of these results. It is clear that the some method is necessary to mitigate track coalescence, which has been shown to cause problems with methods such as GNN, JPDA, and the coupled form of JPDA, namely JPDAC.[7, 9, 10] Blom and Bloem[10] presented JPDA*, which is an extension of JPDA and designed to avoid track coalescence. Although successful in many regimes, this method was particularly susceptible to track swap. A direct comparison to JPDA* is not done here and would prove to be an interesting exercise, however, the defection mitigation presented here is similar to that of JPDA* with delayed decision-making.

Previous studies have compared the ISE reduction method to other reduction methods such as Salmond's clustering filters and direct pruning of low probability hypotheses.[1, 2] A minor extension to these studies is shown here to determine if the two-target case presented different overall trends than those previously discovered and to explore the affects that correlation monitoring might have on performance. Table 4 shows the track life averaged over the 100 Monte Carlo runs for two of the scenarios with the maximum time steps set at 200 per run. As expected, with only 10 hypotheses allowed for the reduced Gaussian mixture, the Salmond clustering filter performs about the same as the ISE method. Both substantially outperform pruning, however, the pruning algorithm is less computationally intensive.

| Scenario | Dynamics | ISE_C_D | ISE_C |
|---|---|---|---|
| 1 | Low | 0.5 | 9.9 |
| 1 | High | 0.3 | 43 |
| 2 | Low | 0 | 0 |
| 2 | High | 0 | 2.8 |
| 3 | Low | 2.9 | 7.6 |
| 3 | High | 0.2 | 36.2 |
| 4 | Low | 0 | 0 |
| 4 | High | 0 | 0 |

**Table 3.** Percent Time in Track Coalescence - 10 mixture reduction components

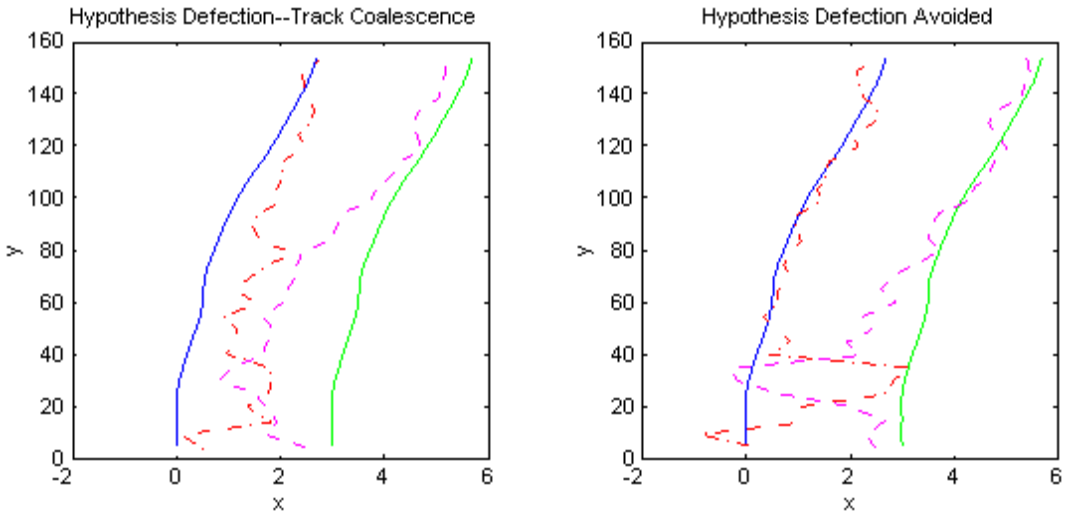


**Figure 2.** Track coalescence due to hypothesis defection

In scenario 1, it is important to note the apparent drop in track life performance for the ISE with correlation. This may appear to be counterintuitive since modelling the correlation is assumed to enhance performance. As mentioned previously, we are modelling the correlation due to the joint observation, not the correlation between the targets' dynamics noises. This has created a modelling mismatch that is significant in the case of scenario 1 as shown in Table 4 and results in degraded performance. It would be difficult to predict how the dynamics noises would be correlated in reality, so the choice to simply model the observation correlation is a reasonable approach. This result provides a clear argument for the use of group tracking of closely spaced targets and for directly modelling dynamics noise coupling if targets must be tracked individually.

Table 5 shows the number of runs out of 100 in which a swap occurred for each of the scenarios. The algorithms implemented include (track defection logic was active in all cases):

- ISE - MISER without correlation or IFF measurements
- ISE_I - MISER with IFF only

| Scenario | Dynamics Noise | Prune | Salmond | ISE_C | ISE |
|---|---|---|---|---|---|
| 1 | High | 27.02 | 55.58 | *25.79* | 62.86 |
| 4 | High | 25.76 | 46.57 | 46.01 | 47.99 |

**Table 4.** Track Life - 10 mixture reduction components, 200 time steps

| Scenario | Dynamics Noise | ISE | ISE_I | ISE_C | ISE_IC |
|---|---|---|---|---|---|
| 1 | Low | 52 | 45 | 4 | 1 |
| 1 | High | 35 | 46 | 30 | 26 |
| 2 | Low | 1 | 1 | 1 | 1 |
| 2 | High | 30 | 17 | 15 | 14 |
| 3 | Low | 1 | 1 | 0 | 0 |
| 3 | High | 42 | 17 | 28 | 16 |
| 4 | Low | 0 | 0 | 0 | 0 |
| 4 | High | 0 | 0 | 0 | 0 |

**Table 5.** Total Number of Track Swaps - 10 mixture reduction components

- ISE_C - MISER with correlation only
- ISE_IC - MISER with IFF and correlation

The data reveals that under certain conditions track swapping can be mitigated by exploiting the correlation between targets via the joint probability array. In particular, with two closely spaced targets travelling in formation (scenario 1, low dynamics) the number of swaps is impressively reduced by modelling correlation between targets. The impact is less significant when the process noise is increased and the target trajectories become very dynamic, where both tracks are struggling to stay locked on either target, leading to a high degree of swapping. The best result is when both correlation and IFF information are incorporated to best resolve track to target ambiguity, although the correlation does not appear to increase the improvement offered by the IFF measurement. As the target separation increases and with higher dynamics noise (scenario 2 versus scenario 1), the dependency between targets is reduced and this naturally results in a less significant but still 2 to 1 improvement due to correlation monitoring. This is clearly expected: if the targets are further apart, or close together for a shorter period of time, then the natural correlation will be smaller, and the benefit of representing it will be less.

Similar results are seen in scenario 3 where the targets cross in the midst of high dynamics noise. At first glance, the culprit for the large number of swaps appears to be the high dynamics noise, but scenario 4 results rebuke this idea with no swaps occurring under all methods shown. The distinction is that under scenario 4 the targets begin far apart and are only close together for a brief period of time, allowing the tracks to maintain continuity. In contrast, the targets in scenario 3 are close together for a longer period of time such that track to target continuity is more difficult to maintain and as the targets cross, the tracks readily swap. The correlation provides a near 2 to 1 reduction in swapping, but the real saving grace is the ability to exploit the IFF information. Scenario 3 illustrates that correlation combined with IFF is not significantly better than IFF alone. In fact, the IFF measurement information dominates the performance as compared to the correlation monitoring. When the targets cross slowly with very similar velocity vectors, the uncertainty in identity becomes very large. This uncertainty can be represented better with correlation than without, but it cannot be resolved: an identity measurement allows it to be resolved.

Finally, track swap is not an issue in all of the low dynamics noise cases except for scenario 1 (closely spaced targets in formation). It was not surprising to find that RMS position error did not vary significantly for each of the implementations of the MISER algorithm. For instance, the RMS for scenario 1, low dynamics noise varied from ISE_IC=0.7926 to ISE=0.8328. Similar results were found in all test cases.

## 4. CONCLUSION

This paper has demonstrated a multiple target extension of the ISE-based mixture reduction technique.[1–3] The efficient representation of correlation between targets maintained by the algorithm was found to substantially reduce track swap in most circumstances. Cases in which the targets were close together for extended periods of time demonstrated that the uncertainty in target identity was severe enough that the efficient representation of the uncertainty was not inadequate to resolve the uncertainty, and that additional measurements of target

identity were also necessary. An *ad hoc* method was incorporated to prevent track coalescence in the presence of hypothesis defection.

Although the apparent result that modelling correlation between targets reduces track life in certain circumstances requires further investigation, the distinction between correlation due to joint observation and correlation due to coupled dynamics processes appears to provide an adequate explanation. This result has surprising implications to systems attempting to track targets in formation: modelling the correlation due to the joint observation process while neglecting the correlation due to the dependent dynamics processes may harm some aspects of performance as compared to the marginalized representation. This reinforces the necessity of the group tracking approach for tracking closely-spaced targets, and suggests that the process noise dependency should be modelled explicitly in applications requiring resolution of individual targets. Future research directions include incorporating track initiation and deletion logic to the MISER algorithm and techniques such as the Interacting Multiple Model (IMM) filter for maneuvering targets.[7]

## DISCLAIMER

The views expressed in this article are those of the authors and do not reflect the official policy or position of the United States Air Force, the Department of Defense, or the U.S. Government.

## REFERENCES


1. J. L. Williams, "Gaussian mixture reduction for tracking multiple maneuvering targets in clutter," Master's thesis, Air Force Institute of Technology, Wright-Patterson Air Force Base, OH, 2003. Available for download at http://handle.dtic.mil/100.2/ADA415317.
2. J. L. Williams and P. S. Maybeck, "Cost-function-based gaussian mixture reduction for target tracking," in *Proceedings of the Sixth International Conference of Information Fusion*, pp. 1047–1054, International Society of Information Fusion, (Cairns, Australia), July 2003.
3. J. L. Williams and P. S. Maybeck, "Cost-function-based hypothesis control techniques for multiple hypothesis tracking," *SPIE Signal and Data Processing of Small Targets* **5428**, April 2004.
4. S. Blackman, R. Dempster, and T. Nichols, "Application of multiple hypothesis tracking to multiradar air defense systems," *Multisensor Multitarget Data Fusion, Tracking and Identification Techniques for Guidance and Control Applications* **NATO AGARD AG-337**, pp. 96–120, October 1996.
5. L. Y. Pao, "Multisensor multitarget mixture reduction algorithms for tracking," *Journal of Guidance, Control, and Dynamics* **17**, pp. 1205–1211, November–December 1994.
6. P. S. Maybeck, *Stochastic Models, Estimation, and Control*, vol. Volume 2, Navtech, Arlington, VA, 1994.
7. Y. Bar-Shalom and X.-R. Li, *Multitarget-Multisensor Tracking: Principles and Techniques*, YBS Publishing, Storrs, CT, 1995.
8. P. S. Maybeck, *Stochastic Models, Estimation, and Control*, vol. Volume 1, Navtech, Arlington, VA, 1994.
9. S. S. Blackman and R. Popoli, *Design and Analysis of Modern Tracking Systems*, Artech House, Norwood, MA, 1999.
10. H. A. Blom and E. A. Bloem, "Probabilistic data association avoiding track coalescence," *IEEE Transactions on Automatic Control* **45**, pp. 247–259, February 2000.
11. D. J. Salmond, "Mixture reduction algorithms for uncertain tracking," Tech. Rep. 88004, Royal Aerospace Establishment, Farnborough, UK, January 1988. DTIC Number ADA197641.